

# Ultracold collisions of metastable helium atoms

P.J. Leo

*Atomic Physics Division, National Institute of Standards and Technology, Gaithersburg,  
Maryland 20899*

V. Venturi\* and I.B. Whittingham

*School of Mathematical and Physical Sciences, James Cook University, Townsville 4811, Australia*

J. F. Babb

*Institute for Theoretical Atomic and Molecular Physics,  
Harvard-Smithsonian Center for Astrophysics,  
60 Garden Street, Cambridge, MA 02138*

(November 2, 2018)

## Abstract

We report scattering lengths for the  $^1\Sigma_g^+$ ,  $^3\Sigma_u^+$  and  $^5\Sigma_g^+$  adiabatic molecular potentials relevant to collisions of two metastable  $2^3S$  helium atoms as a function of the uncertainty in these potentials. These scattering lengths are used to calculate experimentally observable scattering lengths, elastic cross sections and inelastic rates for any combination of states of the colliding atoms, at temperatures where the Wigner threshold approximation is valid.

PACS numbers: 03.75.Fi, 32.10.Hq, 32.80.Dz, 32.80Pj, 33.15.Pw, 34.20Cf, 34.50.-s

Typeset using REVTeX

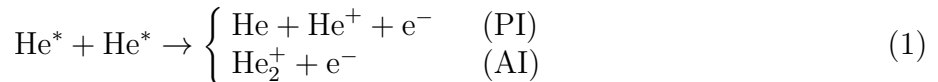
---

\*Present address: Department of Computing Science, Glasgow University, Glasgow G12 8QQ, UK

## I. INTRODUCTION

Metastable helium has been the subject of many experimental investigations at cold and ultracold temperatures. These include various methods of laser cooling [1–8] and trapping [9–13], production of an intense beam [14–16], optical collisions in magneto-optical traps and measurements of two-body trap loss rates, including that due to Penning ionization [17–25], photoassociation spectroscopy [26] and magnetostatic trapping [27]. There have also been several theoretical studies [29–34]. Much of this interest has been stimulated by the prospect of obtaining a Bose-Einstein condensate with spin-polarized metastable helium  $2^3S$  atoms [9,12,22,27,28,32,33]; a quest successfully realized very recently [35,36].

The Penning ionization (PI) and associative ionization (AI) processes,



have high threshold rates in an unpolarized gas and limit the achievable density of trapped atoms. Here we denote a  $\text{He}(2^3S)$  atom by the symbol  $\text{He}^*$ . However, these autoionization processes are spin-forbidden and suppressed [33,34] from the spin-polarized state and only via the weak spin-dipole interaction can such processes occur. Consequently, a sufficient number of spin-polarized metastable atoms should remain trapped. In addition, the scattering length associated with the quintet potential, which controls the collision dynamics of spin-polarized metastable helium atoms, is predicted to be large and positive, a necessary requirement for a stable Bose-Einstein condensate. Although some theoretical studies [31–33] have estimated the scattering length associated with the quintet potential to be large and positive, no detailed study of the scattering lengths for metastable helium has been previously undertaken.

In this present investigation we calculate not only the possible ranges of values for the scattering lengths directly associated with the molecular potentials, but also experimentally observable scattering lengths, elastic cross sections and inelastic rate constants over a range of scattering lengths and temperatures for collisions of metastable helium atoms in the presence of a magnetic field. Measurement of cross sections or rates should then provide information on the scattering lengths and hence the potentials.

For this theoretical investigation we have chosen to simulate the Penning and associative ionization processes that occur at small internuclear separations from the singlet and triplet molecular states by a complex optical potential. The complex interaction potentials then have the form  ${}^{2S+1}V(R) - \frac{1}{2}i{}^{2S+1}\Gamma(R)$ , where  $R$  is the internuclear separation of the two atoms,  ${}^{2S+1}V(R)$  is the usual adiabatic molecular potential for the molecular state  ${}^{2S+1}\Sigma_{g,u}^+$  with total spin  $S$ , and  ${}^{2S+1}\Gamma(R)$  is the corresponding total autoionization width representing flux loss due to the ionization processes. Since the Penning and associative ionization processes are spin-forbidden from the quintet state,  ${}^5\Gamma(R) = 0$ .

In the absence of spectroscopic data which could be used to obtain high accuracy potentials, the adiabatic molecular potentials required in this investigation for the  ${}^1\Sigma_g^+$ ,  ${}^3\Sigma_u^+$  and  ${}^5\Sigma_g^+$  molecular states were constructed using data from various sources. The long-range interaction potential was described by a multipole expansion of the form  $-C_6/R^6 - C_8/R^8 - C_{10}/R^{10}$  using the most accurate dispersion coefficients available for the  $\text{He}(2^3S)\text{--He}(2^3S)$  interaction ( $C_6 = 3276.680$ ,  $C_8 = 210566.55$ ,  $C_{10} = 21786760$  au)

[37]. The short-range  $^1\Sigma_g^+$  and  $^3\Sigma_u^+$  molecular potentials and their corresponding autoionization widths for Penning and associative ionization [38] were obtained from Müller *et al.* [38], while the short-range  $^5\Sigma_g^+$  molecular potential was taken from Stärck and Meyer [39]. The  $^5\Sigma_g^+$  potential was reported with an uncertainty of 0.5% in the repulsive part of the potential and 1% in the attractive part of the potential.

The molecular potentials for metastable helium were constructed by fitting the three short-range potentials smoothly onto the long-range dispersion interaction around  $\approx 20 a_0$  by interpolation through this region using an Akima spline fitted to  $R^6 {}^{2S+1}V(R)$ . The uncertainties in the short-range potentials, the procedure used to connect these to the long-range potential, and the form used for the autoionization widths lead to uncertainties in the scattering lengths for the  $^1\Sigma_g^+$ ,  $^3\Sigma_u^+$  and  $^5\Sigma_g^+$  potentials and subsequently to the ultra-cold scattering properties of metastable helium atoms. To determine the extent of these uncertainties we vary the short-range potentials by  $\pm 2.5\%$  for five different interaction potentials which use different methods to connect the long-range and short-range potentials or have different forms of the autoionization widths. Since there is no available experimental data that can be used to determine the level of accuracy of these short-range potentials, we have chosen to vary them by more than their stated uncertainty to ensure that we obtain conservative estimates for the range of scattering lengths.

The first of these potentials, labeled (A), uses the analytic short-range  $^5\Sigma_g^+$  potential fitted smoothly onto the long-range potential at  $R \approx 20 a_0$ . The numerical  $^1\Sigma_g^+$  and  $^3\Sigma_u^+$  molecular potentials of Ref. [38] are used for  $R < 11.5 a_0$  and for larger  $R$ , where the electronic structure calculations become inaccurate, we replace the potentials by  $^5V(R) - V_{\text{exch}}(R)$ . The exchange term has the form [40]  $V_{\text{exch}}(R) = A_{2S+1}R^\gamma \exp(-\beta R)$ , where [40]  $\gamma = 4.91249$ ,  $\beta = 1.183933$ ,  $A_1 = 6.3245 \times 10^{-3}$  and  $A_3 = 4.6317 \times 10^{-3}$ . The autoionization widths  ${}^{2S+1}\Gamma_M(R)$  of Ref. [38] were used to represent the Penning and associative ionization processes.

Potential (B) is identical to (A) except that the short-range  $^5\Sigma_g^+$  form is fitted to the long-range potential at  $R \approx 35 a_0$ . Potential (C) is identical to (A) except that the exchange term has the form  $V_{\text{exch}}(R) = A_{2S+1} \exp(-\beta R)$  with  $\beta = 0.704921$ ,  $A_1 = 4.29808$  and  $A_3 = 3.14764$ . Potentials (D) and (E) are identical to (A) but employ different forms for the autoionization widths. The autoionization width  $\Gamma_{\text{GMS}}(R) = 0.3 \exp(-R/1.086)$ , given by Garrison *et al.* [41], is used in (D). This autoionization width has a steeper exponential form which doesn't dampen at small internuclear separations like  $^1\Gamma_M(R)$  or  $^3\Gamma_M(R)$ . Potential (E) uses another alternative form of the autoionization widths which was arbitrarily constructed to assess the sensitivity of the calculated results to the form of  $\Gamma(R)$  and is given by:

$$\Gamma(R) = \begin{cases} \Gamma_{\text{GMS}}(R) + (R - 6.5)^2 e^{-0.75R}, & \text{for } R \leq 6.5 \\ \Gamma_{\text{GMS}}(R), & \text{for } R > 6.5. \end{cases} \quad (2)$$

All the molecular potentials considered have the same long-range form since the uncertainties in the long-range multipole potential were found to have a negligible effect on the scattering lengths. The real parts of the potentials (A) to (E) with unmodified short-range forms possess the same number of bound states, calculated to be 28 for  $^1\Sigma_g^+$ , 27 for  $^3\Sigma_u^+$  and 15 for  $^5\Sigma_g^+$ .

## II. SCATTERING LENGTHS ASSOCIATED WITH THE MOLECULAR POTENTIALS

The scattering lengths for the  $^1\Sigma_g^+$ ,  $^3\Sigma_u^+$  and  $^5\Sigma_g^+$  molecular potentials were obtained by solving a single channel radial Schrödinger equation of the form,

$$\left\{ \frac{d^2}{dR^2} - \frac{l(l+1)}{R^2} - [{}^{2S+1}V(R) - \frac{1}{2}i{}^{2S+1}\Gamma(R)] + k^2 \right\} u_{S,l}(k, R) = 0 \quad (3)$$

in the limit where  $k \rightarrow 0$ . Here  $k = \sqrt{2\mu E/\hbar^2}$ ,  $\mu$  is the reduced mass of the atomic system,  $E$  is the total energy of the system and  $l$  is the relative rotational angular momentum. As a result of the complex interaction potential, the scattering equation (3) and the wavefunctions  $u_{S,l}(k, R)$  are complex. Solution of this equation allowing for the non-unitarity of the Hamiltonian, and subsequent fitting to free-field boundary conditions, provides a complex K-matrix and corresponding non-unitary S-matrix ( $S_S$ ), as described previously [33]. The complex phase shift  $\eta_S$ , defined by  $S_S = \exp(i2\eta_S)$ , can then be used to calculate the complex scattering lengths  $a_{2S+1} = a_{2S+1}^{\text{re}} + ia_{2S+1}^{\text{im}}$  for each molecular state  ${}^{2S+1}\Sigma_{g,u}^+$ :

$$\begin{aligned} a_{2S+1}^{\text{re}} &= -\frac{1}{2k} \tan^{-1} \left( \frac{S_S^{\text{im}}}{S_S^{\text{re}}} \right) \\ a_{2S+1}^{\text{im}} &= -\frac{\ln(S_S S_S^\dagger)}{4k}, \end{aligned} \quad (4)$$

where the scattering lengths are defined by  $\eta_S = -k a_{2S+1}^*$  and the superscripts ‘re’ and ‘im’ denote real and imaginary components, respectively. This definition means that  $+ia_{2S+1}^{\text{im}}$  represents a loss process.

The scattering lengths for the three molecular states were calculated as a function of the percentage variation in the corresponding short-range molecular potential for the five potential cases (A) to (E) and are displayed in Fig. 1. For the  $a_5$  scattering length only the results for potential (A) are plotted because the  $^5\Sigma_g^+$  potentials are identical for potential cases (A), (C), (D) and (E) and the results obtained with potential (B) differed by less than 5%. The  $a_5$  scattering length has no imaginary component since the Penning process is spin-forbidden from the  $S = 2$  molecular state. Of particular interest is the resonance in  $a_5$  at a percentage variation of  $\approx 1.875$  where the short-range potential is made sufficiently shallow that a bound state is removed from the  $^5\Sigma_g^+$  potential. For percentage variations  $> 1.875$  it is found that  $a_5$  is negative in contradiction to recent experimental evidence that  $a_5$  is large and positive [35,36]. With potentials (A) and (B) the scattering lengths  $a_1$  and  $a_3$  were nearly identical and are denoted by a single solid curve.

The scattering lengths associated with the molecular potentials are not observable experimentally, with the exception of  $a_5$ , which is approximately equal to the scattering length for the spin-polarized state. However, these scattering lengths provide unique parameterization of the  $^1\Sigma_g^+$ ,  $^3\Sigma_u^+$  and  $^5\Sigma_g^+$  potentials, from which the threshold scattering properties of metastable helium atoms can be obtained. Of more practical interest are the scattering lengths for collisions between atoms in given atomic states in the presence of a magnetic field.

### III. COLLISIONS IN THE PRESENCE OF A MAGNETIC FIELD

To study collisions in the presence of a magnetic field a full multichannel scattering calculation must be undertaken in which the total Hamiltonian describing the two-body collision includes the spin-orbit, Zeeman and spin-dipole interactions in addition to the usual radial and rotational kinetic energy operators of the two atoms and the electronic Hamiltonian of the quasimolecule formed during the collision. The details of such a quantum-mechanical multichannel scattering model for metastable helium is described elsewhere [33]. In brief, we perform the present calculations for atoms in initial atomic states  $\alpha$  and  $\beta$ , including both  $s$  and  $d$ -waves, and calculate the full non-unitary S-matrix which has elements  $S_{\alpha,\beta,l;\alpha',\beta',l'}$ . Here we let  $\alpha$  and  $\beta$  denote the atomic states  $(s, m_s)$ , where  $m_s$  is the space-fixed projection of the spin  $s$  for an individual atom.

For collision energies up to  $100 \mu\text{K}$  the contributions of entrance  $p$  and  $d$ -waves are negligible (note that due to symmetrization  $p$ -waves only contribute in collisions between atoms in different atomic states), so that only the  $s$ -wave entrance channel  $[\alpha, \beta], l = 0$  needs to be considered. The elastic cross section  $\sigma_{\alpha,\beta}^{\text{el}}$  and inelastic rate  $K_{\alpha,\beta}^{\text{inel}}$  are then given by [42]

$$\begin{aligned}\sigma_{\alpha,\beta}^{\text{el}} &= \frac{\pi}{k^2} |1 - S_{\alpha,\beta,l=0;\alpha,\beta,l=0}|^2 \\ K_{\alpha,\beta}^{\text{inel}} &= \frac{v\pi}{k^2} \left(1 - |S_{\alpha,\beta,l=0;\alpha,\beta,l=0}|^2\right),\end{aligned}\tag{5}$$

where  $v$  is the relative atomic velocity. In the Wigner threshold region ( $ka \ll 1$ ) one can define the scattering lengths using  $\eta_{\alpha,\beta} = -ka_{\alpha,\beta}^*$  and obtain expressions for the observable scattering lengths  $a_{\alpha,\beta}$  by replacing  $S_S$  with the matrix element  $S_{\alpha,\beta,l=0;\alpha,\beta,l=0}$  in Eq. (4). The elastic cross sections and inelastic rates can then be obtained using

$$\begin{aligned}\sigma_{\alpha,\beta}^{\text{el}} &= 4\pi \left[ (a_{\alpha,\beta}^{\text{re}})^2 + (a_{\alpha,\beta}^{\text{im}})^2 \right] \\ K_{\alpha,\beta}^{\text{inel}} &= 4\pi a_{\alpha,\beta}^{\text{im}}/k.\end{aligned}\tag{6}$$

The inelastic rate  $K_{\alpha,\beta}^{\text{inel}}$  includes both contributions from the flux loss due to Penning ionization and that due to the atoms exiting in different atomic states. Since we calculate the full S-matrix, the contributions of these two processes can be easily separated. We note that for  $(1, 1) + (1, 1)$ ,  $(1, 1) + (1, 0)$ ,  $(1, -1) + (1, -1)$  or  $(1, -1) + (1, 0)$  collisions, where the total projection of the spin ( $M$ ) is non-zero, the collision is dominated by the  ${}^5\Sigma_g^+$  potential. This is because parity considerations associate the  ${}^3\Sigma_u^+$  potential with odd partial waves, and cold collisions are dominated by  $s$  wave collisions, and the  ${}^1\Sigma_g^+$  potential can only contribute when  $M = 0$ . Hence inelastic processes can only occur via the weak relativistic spin-dipole interaction. The scattering lengths for these states are then almost identical to  $a_5$  but with a small imaginary component. The properties of  $(1, 1) + (1, 1)$  collisions were investigated in detail in a previous paper [33]. The inelastic rates for  $(1, 0) + (1, 0)$  and  $(1, 1) + (1, -1)$  collisions, from which ionization can occur directly via strong exchange forces, are much larger and dominate the total inelastic rate for an unpolarized gas.

The  $(1, 0) + (1, 0)$  and  $(1, 1) + (1, -1)$  inelastic rates contain two different contributions. The first is due to exothermic inelastic processes which includes the Penning rate  $K_{\alpha,\beta}^{\text{P}}$  and the much smaller collision rate for exothermic fine-structure changing collisions  $K_{\alpha,\beta}^{\text{ex}}$ . The second is the rate for degenerate fine-structure changing collisions  $K_{\alpha,\beta}^{\text{deg}}$ . For example,

in ultracold  $(1, 0) + (1, 0)$  collisions, the entrance channel  $[(1, 0) + (1, 0)], l = 0$  can decay exothermically to the three channels  $[(1, -1) + (1, -1)], l = 2$ ;  $[(1, 0) + (1, -1)], l = 2$  and the Penning channel, and to the two degenerate channels  $[(1, 1) + (1, -1)], l = 0$  and  $[(1, 1) + (1, -1)], l = 2$ . The flux loss to the degenerate  $d$ -wave exit channels or exothermic  $d$ -wave exit channels (ie  $K^P$ ) only occurs via weak spin-dipole forces and is at least 3 orders of magnitude smaller than that lost to the Penning channel or to degenerate  $l = 0$  exit channels that occurs through strong exchange forces. Importantly, exothermic and degenerate inelastic processes exhibit different threshold properties. Exothermic inelastic rates tend to a constant in the Wigner threshold region whereas degenerate inelastic rates fall off as  $1/k$  since, as for elastic processes, the incident and final wave number are identical. To represent these separate threshold behaviors in the inelastic rates, we write  $a_{\alpha,\beta}^{\text{im}} = a_{\alpha,\beta}^{\text{im ex}} + k a_{\alpha,\beta}^{\text{im deg}}$ . The slope and intercept of  $\ln(S_{\alpha,\beta,l=0;\alpha,\beta,l=0} S_{\alpha,\beta,l=0;\alpha,\beta,l=0}^\dagger)/4k$  vs  $k$ , for  $k$  in the Wigner threshold region, then gives the degenerate and exothermic scattering lengths  $a_{\alpha,\beta}^{\text{im deg}}$  and  $a_{\alpha,\beta}^{\text{im ex}}$ , respectively.

We have calculated these imaginary and the real scattering lengths for all possible collision processes in spin-polarized metastable helium for the five different potentials under investigation. From these calculated scattering lengths one can use Eq. (6) to calculate the partial rates or the total rates in an unpolarized gas at temperatures where the Wigner threshold approximation is valid. The scattering lengths are calculated assuming a magnetic field of 10 Gauss, however we find only a weak dependence on the magnetic field and results for fields in the range 0 to 20 Gauss differ by less than 1%. The scattering lengths can be used to calculate the rates and cross sections up to typically  $\approx 100 \mu\text{K}$ , except where the scattering lengths become  $> 1000 a_0$ .

Scattering lengths for  $(1, 0) + (1, 0)$  and  $(1, 1) + (1, -1)$  collisions (with  $s$  and  $d$ -waves) depend on both the  ${}^5\Sigma_g^+$  and  ${}^1\Sigma_g^+$  potentials and so their scattering lengths are a function of both the percentage variation of the short-range  ${}^5\Sigma_g^+$  and  ${}^1\Sigma_g^+$  potentials for potential cases (A) to (E). However, we find that for a fixed percentage variation of the  ${}^5\Sigma_g^+$  potential, the uncertainty in the scattering lengths induced by varying the short-range  ${}^1\Sigma_g^+$  potential by  $\pm 2.5\%$  is similar to that calculated by fixing the percentage variation in the  ${}^1\Sigma_g^+$  potential to zero and using the five different potential cases (A) to (E). In all instances the percentage variation in the  ${}^5\Sigma_g^+$  potential has the largest effect on the scattering lengths and resulting rates. The  $(1, 1) + (1, 1)$ ,  $(1, 1) + (1, 0)$ ,  $(1, -1) + (1, -1)$  or  $(1, -1) + (1, 0)$  interactions depend only weakly on the singlet potential via the weak relativistic spin-dipole interaction and we find that varying the short-range  ${}^1\Sigma_g^+$  potential for these collisions produces negligible changes in the scattering length. Therefore we only report scattering lengths as a function of the percentage variation in the  ${}^5\Sigma_g^+$  potential for potential cases (A) to (E), with the understanding that similar uncertainties result in the  $(1, 0) + (1, 0)$  and  $(1, 1) + (1, -1)$  scattering lengths by varying the short-range singlet potential.

Figures 2, 3 and 4 show the real and imaginary components of the scattering lengths for  $(1, 1) + (1, 1)$ ,  $(1, 0) + (1, 0)$  and  $(1, 1) + (1, -1)$  collisions. The real scattering lengths all possess a resonance in the region where a bound state is removed from the  ${}^5\Sigma_g^+$  potential and  $a_5$  goes through  $\pm\infty$ . Similar plots exist for  $(1, 1) + (1, 0)$ ,  $(1, -1) + (1, -1)$  and  $(1, -1) + (1, 0)$  collisions but are almost identical to that shown in Fig. 2 for  $(1, 1) + (1, 1)$  since all are dominated by the  ${}^5\Sigma_g^+$  potential. The underlying  ${}^5\Sigma_g^+$  potentials are identical for potential cases (A), (C), (D) and (E) and we found that  $a_{(1,1),(1,1)}^{\text{re}}$  calculated with these potentials differed from those obtained using potential (B) by less than 2%. These small

differences are not observable on the scale used in Fig. 2 and so for clarity a single solid curve is used to represent  $a_{(1,1),(1,1)}^{\text{re}}$  for the five potential cases. Similarly for  $a_{(1,1),(1,1)}^{\text{imex}}$  the results were identical except for cases (D) and (E) where different forms of the autoionization widths were used, and so we show only results for (A), (D) and (E) potential cases. We note that imaginary scattering lengths for collisions where the total spin projection is non-zero possess no degenerate component and the exothermic contributions are negligible when compared to those for  $(1, 0) + (1, 0)$  and  $(1, 1) + (1, -1)$  collisions where Penning ionization can occur via exchange forces.

For  $(1, 0) + (1, 0)$  and  $(1, 1) + (1, -1)$  collisions the values of  $a^{\text{re}}$  in Fig. 3 were almost identical for the five potential cases and are represented by a single solid curve for  $(1, 0) + (1, 0)$  and a dashed curve for  $(1, 1) + (1, -1)$ . In Fig. 4 we show  $a^{\text{imex}}$  and  $a^{\text{imdeg}}$  for these collisions. The scattering lengths  $a^{\text{imex}}$ , which measure  $K_{\alpha,\beta}^{\text{P}} + K^{\text{ex}}$ , are independent of the percentage variation in the  ${}^5\Sigma_g^+$  potential and thus  $a_5$ , except very near the  $a_5$  resonance where the contribution from  $K_{\alpha,\beta}^{\text{ex}}$  is no longer negligible and a small increase in  $a_{\alpha,\beta}^{\text{imex}}$  is observable. Therefore, the measurement of the ionization signal from trapped metastable helium atoms does not provide information about  $a_5$ , the parameter which is required to make predictions of the formation or properties of a Bose condensate of spin-polarized metastable helium atoms. If  $K_{\alpha,\beta}^{\text{ex}}$  is neglected then a simple examination of the Hamiltonian shows that  $2K_{(1,0),(1,0)}^{\text{P}} = K_{(1,1),(1,-1)}^{\text{P}}$ . We have verified that this relation is valid to better than 1% and so in Fig. 4 we plot results for  $a_{(1,0),(1,0)}^{\text{imex}}$  for the five potential cases with the understanding that  $2a_{(1,0),(1,0)}^{\text{imex}} = a_{(1,1),(1,-1)}^{\text{imex}}$ .

The curves labeled  $a^{\text{imdeg}}$  in Fig. 4 provide the degenerate temperature-dependent inelastic rates for either  $(1, 0) + (1, 0) \rightarrow (1, 1) + (1, -1)$  or  $(1, 1) + (1, -1) \rightarrow (1, 0) + (1, 0)$ . These equal, exchange-dominated rates strongly mix the  $(1, 1)$ ,  $(1, 0)$  and  $(1, -1)$  atoms and are equal to, or larger than,  $K^{\text{P}}$  at temperatures greater than  $500 \mu\text{K}$  or when the quintet potential is near resonance. Of the potentials tested only those with very different exchange terms provided significantly different results and consequently  $a^{\text{imdeg}}$  for potentials (A), (B), (D) and (E) were nearly identical. For convenience only  $a_{(1,0),(1,0)}^{\text{imdeg}}$  for potentials (A) and (C) have been plotted in Fig.4.

The elastic cross section depends on the real and imaginary scattering lengths and its measurement in a spin-polarized or unpolarized gas may provide useful information on  $a_5$ . In Figs. 5–8 we provide the thermally-averaged total elastic cross sections and Penning ionization rates for  $(1, 1) + (1, 1)$  collisions and for an unpolarized gas calculated using Potential (A). Also shown are results for  $1 \mu\text{K}$  and  $500 \mu\text{K}$  calculated from the scattering lengths using Eq.(6). In general the results obtained using Eq.(6) for temperatures up to  $100 \mu\text{K}$  are identical to the thermally-averaged results whereas at higher temperatures, outside the Wigner regime, the use of scattering lengths is inappropriate and thermal averaging is required. The rate equations

$$\begin{aligned} \frac{\partial n_\alpha}{\partial t} &= K_{\alpha,\alpha}^{\text{inel}} n_\alpha^2 \\ \frac{\partial n_\alpha}{\partial t} &= K_{\alpha,\beta}^{\text{inel}} n_\alpha n_\beta \end{aligned} \quad (7)$$

define our partial rates for, respectively, identical and non-identical atom collisions, where  $n_\alpha$  is the number of colliding atoms in state  $\alpha$  and the superscript ‘inel’ denotes ‘P’, ‘ex’ or

‘deg’. The total thermally-averaged Penning rates and cross sections for an unpolarized gas are obtained assuming an equal population of the  $s = 1$  magnetic substates so that  $n_\alpha = n/3$  and hence

$$\begin{aligned}\frac{\partial n}{\partial t} &= \frac{1}{9} \sum_{\alpha,\beta} \langle K_{\alpha,\beta}^{\text{P}} \rangle n^2 \\ \frac{\partial n}{\partial t} &= \frac{1}{9} \sum_{\alpha,\beta} \frac{\langle v \sigma_{\alpha,\beta}^{\text{inel}} \rangle}{\langle v \rangle} n^2,\end{aligned}\tag{8}$$

where  $\langle \dots \rangle$  denotes the thermal average. In this case the assumption that the magnetic substates are evenly populated in an unpolarized gas is well justified on collisional grounds. At temperatures above  $500 \mu\text{K}$  the degenerate rates  $K^{\text{imdeg}}$  evenly mix  $(1, 1)$ ,  $(1, 0)$  and  $(1, -1)$  atoms. At lower temperatures the Penning rates  $K_{(1,0),(1,0)}^{\text{P}}$  and  $K_{(1,1),(1,-1)}^{\text{P}}$ , which dominate the exothermic inelastic rates, deplete the three different atomic populations  $n_\alpha$  equally since  $2K_{(1,0),(1,0)}^{\text{P}} = K_{(1,1),(1,-1)}^{\text{P}}$  and the collision of  $(1, 0) + (1, 0)$  results in the loss of two  $(1, 0)$  atoms. Here we have neglected the small contribution from spin-dipole processes, that is  $K_{(1,1),(1,-1)}^{\text{ex}}$ , and assume that any initial asymmetry in the populations  $n_\alpha$  due to preparation of the atoms in a light field for instance is small or has become small once the measurement of the collisional rate in the absence of light is performed. The thermally-averaged results were calculated by averaging over a Maxwell-Boltzmann distribution of atomic velocity using 71 velocity nodes which correspond to collision energies in the range  $0.01 \mu\text{K}$  to  $10,000 \mu\text{K}$ . Since the results are for the case (A) potentials, with the percentage variation in the singlet potential set to zero, we estimate from the uncertainties in the scattering lengths that the errors in the elastic cross sections and total inelastic rates are of the order of 10% and 40% respectively. The Penning rates possess a larger uncertainty to account for the percentage variation of the  $^1\Sigma_g$  potential whereas the unpolarized elastic rates, which are dominated by the real scattering lengths belonging to collisions with  $M = 2$  or 1, are controlled only by  $^5\Sigma_g$ .

In an unpolarized gas the  $p$ -waves can contribute in  $(1, 1) + (1, -1)$ ,  $(1, 1) + (1, 0)$  and  $(1, -1) + (1, 0)$  collisions. These contributions to the total thermally-averaged Penning rates were found to be negligible at  $1 \mu\text{K}$ . However the  $p$ -wave contributions increased the total Penning rate (compared to that obtained using only  $s$ -waves) by approximately 7% at  $500 \mu\text{K}$  and 12% at  $1 \text{mK}$ . The  $p$ -waves modified the total elastic cross sections by less than 1% at all temperatures.

For  $(1, 1) + (1, 1)$  collisions (and similarly for  $(1, 1) + (1, 0)$ ,  $(1, -1) + (1, -1)$  or  $(1, -1) + (1, 0)$ ) we observe a resonance in the inelastic rates at a percentage variation of  $+1.875$  due to the resonant enhancement of the exothermic rates. We find that  $K_{\alpha,\beta}^{\text{P}} > K_{\alpha,\beta}^{\text{ex}}$ , indicating that most but not all of the flux leaving the  $[(1, 1) + (1, 1)], l = 0$  entrance channel is subsequently lost through ionization. These rates are much smaller than those from the  $(1, 0) + (1, 0)$  and  $(1, 1) + (1, -1)$  collisions and the total contribution to  $K_{\alpha,\beta}^{\text{P}}$  from  $(1, 1) + (1, 1)$ ,  $(1, 1) + (1, 0)$ ,  $(1, -1) + (1, -1)$  and  $(1, -1) + (1, 0)$  collisions is only observable in Fig. 8 as a small peak at  $+1.875$  in the unpolarized ionization rate.

The total elastic cross sections of an unpolarized or a polarized gas show strong dependences on the form of the  $^5\Sigma_g^+$  potential and provide possible measures of  $a_5$ .



## IV. CONCLUSIONS

The scattering lengths associated with the three molecular potentials relevant to collisions of metastable helium atoms have been reported. The uncertainties in the molecular potentials and autoionization widths have been considered and probable ranges of values given for the scattering lengths for each molecular state. Scattering lengths for collisions involving the various atomic states have also been calculated and related to the elastic cross sections and inelastic collision rates for temperatures in the Wigner threshold region, with the aim of providing a correspondence with experimentally measurable quantities. In particular, it has been shown that measurement of the total elastic cross section in a polarized or unpolarized gas should provide a means of experimentally determining the  $a_5$  scattering length, which is of importance in the attainment of a Bose-Einstein condensate in a gas of spin-polarized metastable helium atoms.

In Fig. 8 we compare the total Penning rates for an unpolarized gas calculated here with those from experiment. Not shown are the theoretical uncertainties of  $\approx 40\%$  which arise from uncertainties in the molecular potentials and in the form of the ionization widths. The total elastic cross sections and Penning rates are consistent with those reported in Ref. [34] where slightly different molecular potentials and ionization widths were used. The experimental results possess uncertainties on the order of 50% which are not shown in Fig. 8. The experimental results correspond to the case of zero magnetic field whereas the theoretical predictions are made for  $B = 10$  G. However the scattering lengths were found to vary by less than 1% over the range 0–20 G which is negligible when compared to these uncertainties that arise from the form of the ionization width. The comparison between theoretical and experimental data is satisfactory given these uncertainties, however the experimental results are consistently higher than the theoretical predictions.

Prior to the submission of this paper, no experimental results or theoretical predictions existed for the scattering lengths, cross sections and rates calculated here for incident atoms in specific states. The  $(1, 1) + (1, 1)$  spin-polarized system has been investigated by Shlyapnikov *et al.* [31,32] and [33] but no (quantitative)  $^5\Sigma_g^+$  scattering lengths were reported. However, during the review of this paper, two measurements of scattering length have been announced;  $377 \pm 189 a_0$  by [35] and  $302 \pm 151 a_0$  by [36]. These measurements, together with measured suppression by a factor of  $> 2 \times 10^3$  for the Penning ionization rate for a spin polarized gas compared to that of an unpolarized gas, are consistent with the current predictions.

Finally, using the scattering lengths reported in this investigation, one can estimate the scattering lengths for the other isotopes of helium by mass scaling the vibrational defect. This is related to the scattering length by [43]

$$a_{2S+1} = - \left. \frac{\partial \nu}{\partial \kappa} \right|_{\kappa \rightarrow 0} \left[ \cot\left(\frac{\pi}{t-2}\right) + \cot(\nu_S(0)) \right], \quad (9)$$

where  $\nu_S(0)$  is the vibrational defect and  $t$  is defined by the leading term  $-C_t/R^t$  in the long-range potential ( $t = 6$  for He). The term  $\left. \frac{\partial \nu}{\partial \kappa} \right|_{\kappa \rightarrow 0}$  is an asymptotic property which depends only on the long-range potential and can be approximated by  $0.956 \times 0.5(2\mu C_6)^{0.25} \approx 35$  for He [44]. To mass scale the vibrational defect we first calculate  $\nu_S(0)$  for  $^4\text{He}$  for a given potential. Since the trigonometric function is periodic, this only gives the fractional part of

the vibrational defect and one must include the multiple of  $n\pi$  where  $n$  is the number of bound states supported by that potential, ie  $\nu_S(0) \rightarrow n\pi + \nu_S(0)$ . This vibrational defect can then be scaled using  $(\mu_x/\mu_4)^{0.5} \times \nu_S(0)$ , to determine the vibrational defect for isotope  $x$ . Here  $\mu_x$  and  $\mu_4$  are the reduced masses of  $^x\text{He}$  and  $^4\text{He}$  respectively.

### ACKNOWLEDGMENTS

VV acknowledges partial support from the Engineering and Physical Sciences Research Council. The Institute for Theoretical Atomic and Molecular Physics is supported by a grant from the NSF to the Harvard College Observatory and the Smithsonian Astrophysical Observatory.

## REFERENCES

- [1] A. Aspect *et al.*, Phys. Rev. Lett. **61**, 826 (1988).
- [2] A. Aspect *et al.*, J. Opt. Soc. Am. B **6**, 2112 (1989).
- [3] N. Morita and M. Kumakura, Jpn. J. App. Phys. **30**, L1678 (1991).
- [4] J. Lawall *et al.*, Phys. Rev. Lett. **73**, 1915 (1994).
- [5] J. Lawall *et al.*, Phys. Rev. Lett. **75**, 4194 (1995).
- [6] W. Rooijackers, W. Hogervorst, and W. Vassen, Phys. Rev. Lett. **74**, 3348 (1995).
- [7] W. Rooijackers, W. Hogervorst, and W. Vassen, Phys. Rev. A **56**, 3083 (1997).
- [8] R. Schumann *et al.*, Phys. Rev. A **59**, 2120 (1999).
- [9] H. Metcalf, J. Opt. Soc. Am. B **6**, 2206 (1989).
- [10] C. Westbrook *et al.*, in *TENICOLS '91, papers presented at Tenth International Conference on Laser Spectroscopy, France, June 1991*, edited by E. G. M. Ducloy and G. Camy (World Scientific, Singapore, 1991), pp. 48–9.
- [11] M. Kumakura and N. Morita, Jpn. J. App. Phys. **31**, L276 (1992).
- [12] W. Vassen, OSA TOPS on Ultracold Atoms and BEC **7**, 20 (1997).
- [13] W. Rooijackers, W. Hogervorst, and W. Vassen, Opt. Commun. **135**, 149 (1997).
- [14] A. Aspect *et al.*, Chem. Phys. **145**, 307 (1990).
- [15] W. Rooijackers, W. Hogervorst, and W. Vassen, Opt. Commun. **123**, 321 (1996).
- [16] M. D. Hoogerland *et al.*, Aust. J. Phys. **49**, 567 (1996).
- [17] F. Bardou *et al.*, Europhys. Lett. **20**, 681 (1992).
- [18] H. C. Mastwijk, J. W. Thomsen, P. van der Straten, and A. Neihaus, Phys. Rev. Lett. **80**, 5516 (1998).
- [19] H. C. Mastwijk, M. van Rijnbach, J. W. Thomsen, P. van der Straten, and A. Neihaus, Euro. Phys. J. D **4**, 131 (1998).
- [20] G. Woestenenk *et al.*, Nuclear Instruments and Methods in Physics Research B **154**, 194 (1999).
- [21] M. Kumakura and N. Morita, Phys. Rev. Lett. **82**, 2848 (1999).
- [22] P. J. J. Tol *et al.*, Phys. Rev. A **60**, R761 (1999).
- [23] A. Browaeys *et al.*, Euro. Phys. J. D **8**, 199 (2000).
- [24] N. Herschbach, P. J. J. Tol, W. Hogervorst, and W. Vassen, Phys. Rev. A **61**, 050702(R) (2000).
- [25] F. Pereira Dos Santos *et al.*, Preprint physics/0103063
- [26] N. Herschbach *et al.*, Phys. Rev. Lett. **84**, 1874 (2000).
- [27] S. Nowak *et al.*, Appl. Phys. B: Lasers Opt. **70**, 1 (2000).
- [28] F. Pereira Dos Santos *et al.*, Preprint physics/0103064
- [29] P. S. Julienne and F. H. Mies, J. Opt. Soc. Am. B **6**, 2257 (1989).
- [30] C. J. Williams and P. S. Julienne, Theory of Penning Ionization of Metastable He, 1992, presented at the Symposium on Cold Atom Collisions, Cambridge, MA, 1992 (unpublished).
- [31] G. V. Shlyapnikov, J. T. M. Walraven, U. M. Rahmanov, and M. W. Reynolds, Phys. Rev. Lett. **73**, 3247 (1994).
- [32] P. O. Fedichev, M. W. Reynolds, U. M. Rahmanov, and G. V. Shlyapnikov, Phys. Rev. A **53**, 1447 (1996).
- [33] V. Venturi, I. B. Whittingham, P. J. Leo, and G. Peach, Phys. Rev. A **60**, 4635 (1999).
- [34] V. Venturi and I. B. Whittingham, Phys. Rev. A **61**, 060703(R) (2000).

- [35] A. Robert *et al.*, *Science* **292**, 461 (2001)
- [36] F. Pereira Dos Santos *et al.*, *Phys. Rev. Lett.* **86**, 3459 (2001)
- [37] Z.-C. Yan and J. F. Babb, *Phys. Rev. A* **58**, 1247 (1998).
- [38] M. W. Müller *et al.*, *Z. Phys. D. - Atoms, Molecules and Clusters* **21**, 89 (1991).
- [39] J. Stärck and W. Meyer, *Chem. Phys. Lett.* **225**, 229 (1994).
- [40] K. T. Tang, J. P. Toennies and C. L. Yui, *Int. Rev. Phys. Chem.* **17**, 363 (1998)
- [41] B. J. Garrison, W. H. Miller and H. F. Schaefer, *J. Comput. Phys.* **59**, 3193 (1973).
- [42] L. D. Landau and E. M. Lifshitz , *Quantum Mechanics*, Vol 3, 3rd ed. (Pergamon Press, Oxford, 1977).
- [43] F. H. Mies *et al.*, *J. Res. Natl. Inst. Stand. Technol.* **101**, 521 (1996).
- [44] G. F. Gribakin and V.V. Flambaum, *Phys. Rev. A* **48**, 546 (1998).

FIGURES

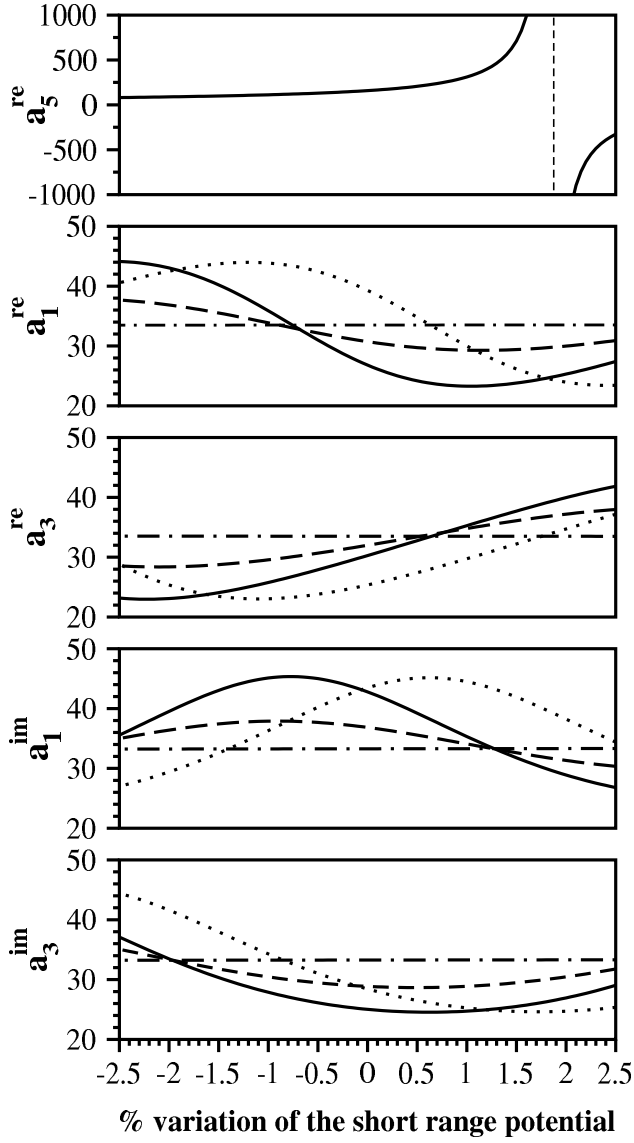


FIG. 1. Real and imaginary components of the scattering lengths  $a_1$ ,  $a_3$  and  $a_5$  plotted against variation in the short-range potential. For  $a_5$  the five potential cases produced similar results and are encompassed by the solid curve with a dashed line to denote the position of the resonance. For  $a_1$  and  $a_3$ , potentials (A) and (B) produced identical results denoted by (—), potential (C) by (···), potential (D) by (- - -) and potential (E) by (- · -).

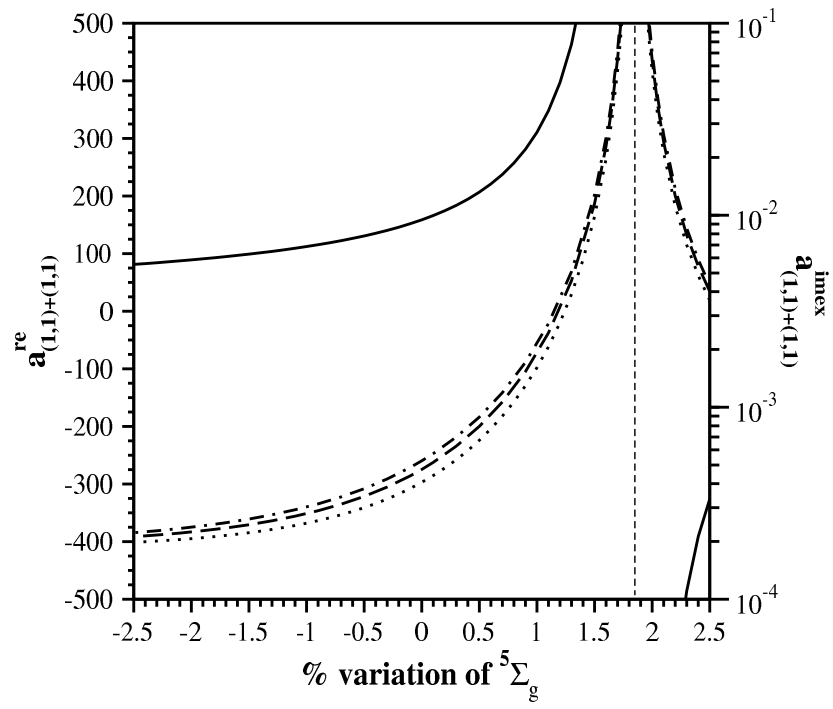


FIG. 2. Complex scattering lengths for  $(1, 1) + (1, 1)$  collisions. The solid line includes the real components of the scattering lengths obtained from all five potential cases. The dashed and dotted lines give the imaginary components of the scattering lengths. Results for potentials (A), (B) and (C) are given by  $(\cdot\cdot\cdot)$ , potential (D) by  $(- - -)$  and potential (E) by  $(- \cdot -)$ .

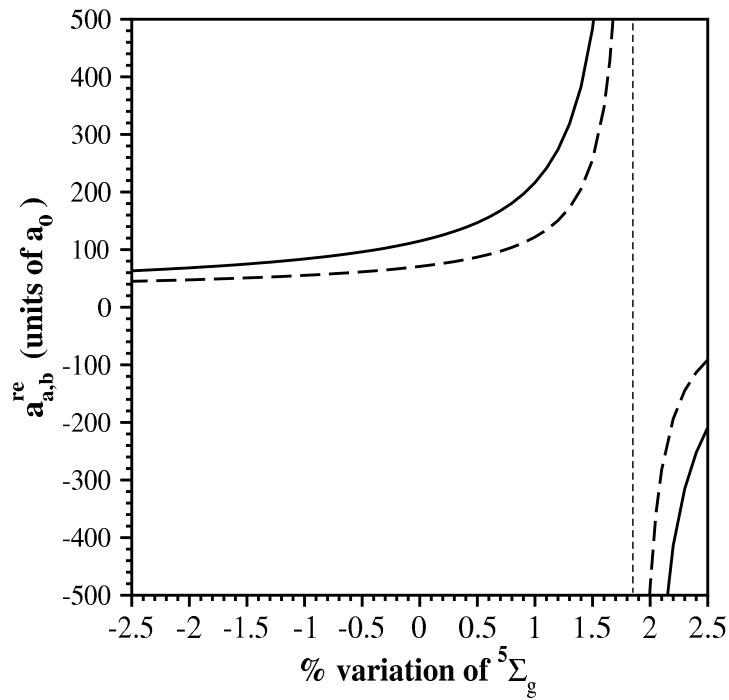


FIG. 3. Real components of the scattering lengths for  $(1,0)+(1,0)$  and  $(1,-1)+(1,1)$  collisions. The solid line represents the results for  $(1,0)+(1,0)$  collisions for all five potential cases, the dashed line includes results for  $(1,-1)+(1,1)$  collisions for all five potential cases.

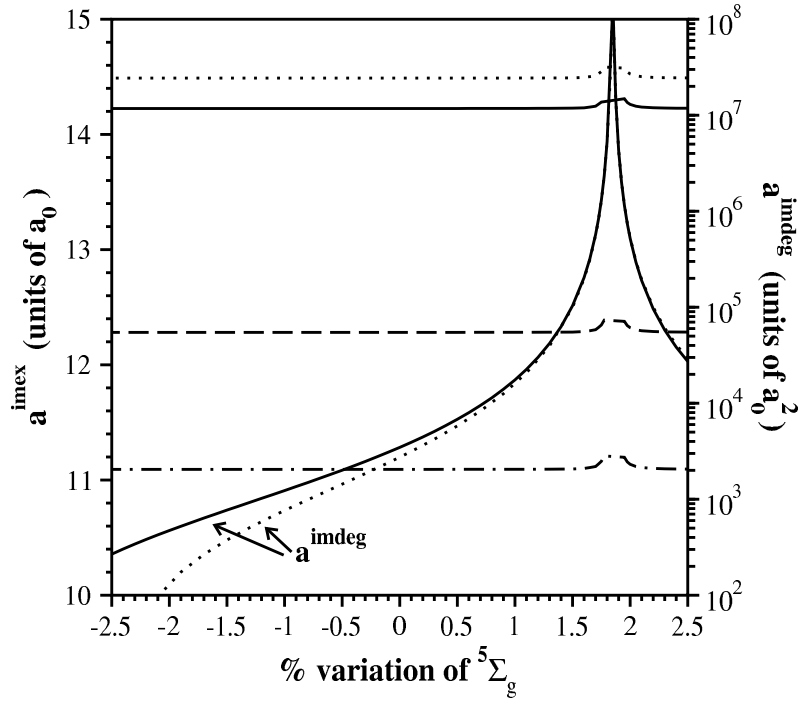


FIG. 4. Imaginary components of the scattering lengths for  $(1,0) + (1,0)$  and  $(1,-1) + (1,1)$  collisions. The near horizontal lines are for  $(1,0) + (1,0)$  collisions with results for potentials (A) and (B) encompassed by the solid curve, potential (C) by  $(\cdots)$ , potential (D) by  $(- - -)$  and potential (E) by  $(- \cdot -)$ . Note that  $2a_{(1,0),(1,0)}^{\text{im ex}} = a_{(1,-1),(1,1)}^{\text{im ex}}$ . The values of  $a^{\text{imdeg}}$  for  $(1,0) + (1,0)$  and  $(1,-1) + (1,1)$  collisions are equal and results for potentials (A), (B), (D) and (E) are encompassed by the solid curve and those for potential (C) by the dotted curve.



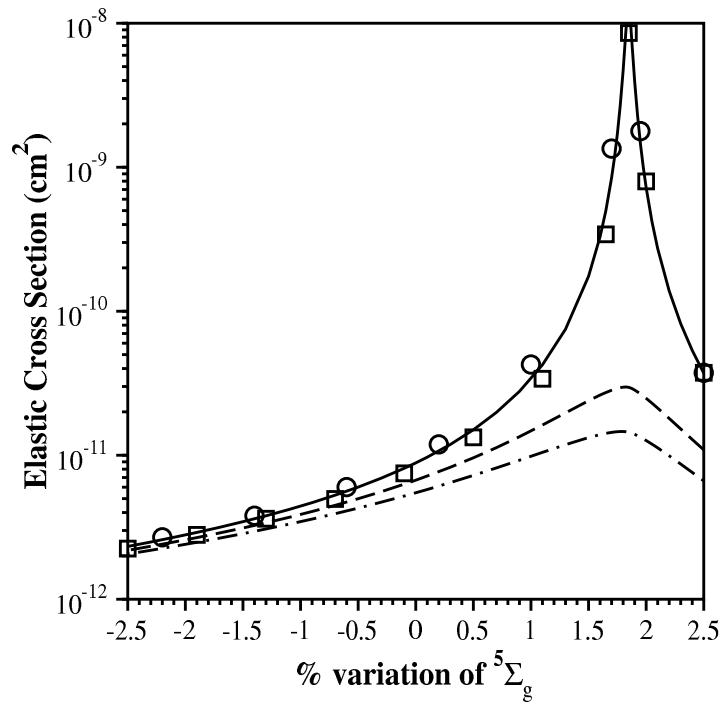


FIG. 5. Thermally-averaged elastic cross section for  $(1, 1) + (1, 1)$  collisions with potential (A) at various temperatures denoted by (—) for  $1 \mu\text{K}$ , (---) for  $500 \mu\text{K}$ , (-.-) for  $1000 \mu\text{K}$ . Results for  $1 \mu\text{K}$  and  $500 \mu\text{K}$  calculated using the scattering lengths are denoted by  $\square$  and  $\circ$  respectively.

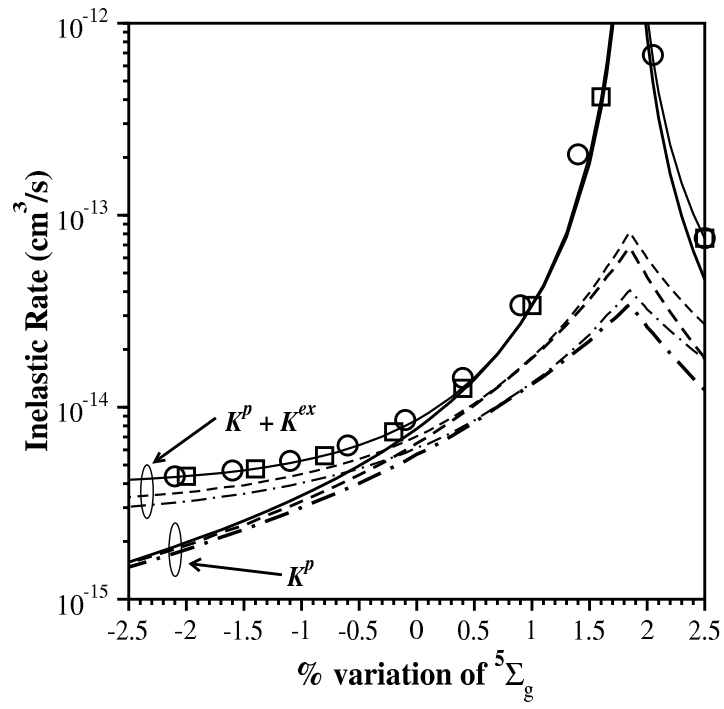


FIG. 6. Thermally-averaged inelastic rates for (1,1) + (1,1) collisions for potential (A) with curves and symbols labeled using the same scheme as in Fig. 5. Thick lines labeled  $K^P$  denote the Penning rate  $K^P$  and the thinner lines labeled  $K^P + K^{ex}$  give the total inelastic rate.

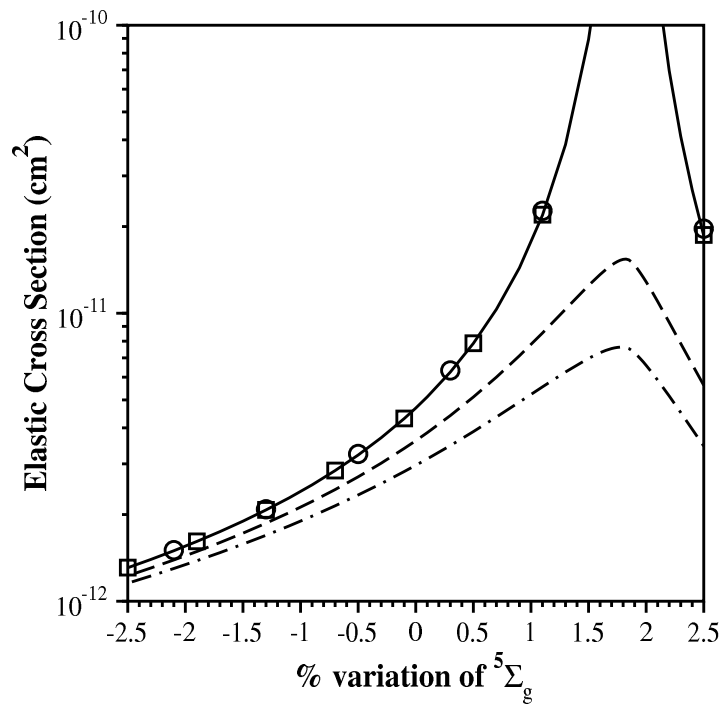


FIG. 7. Thermally-averaged elastic cross sections for an unpolarized gas with curves labeled as per Fig.5.

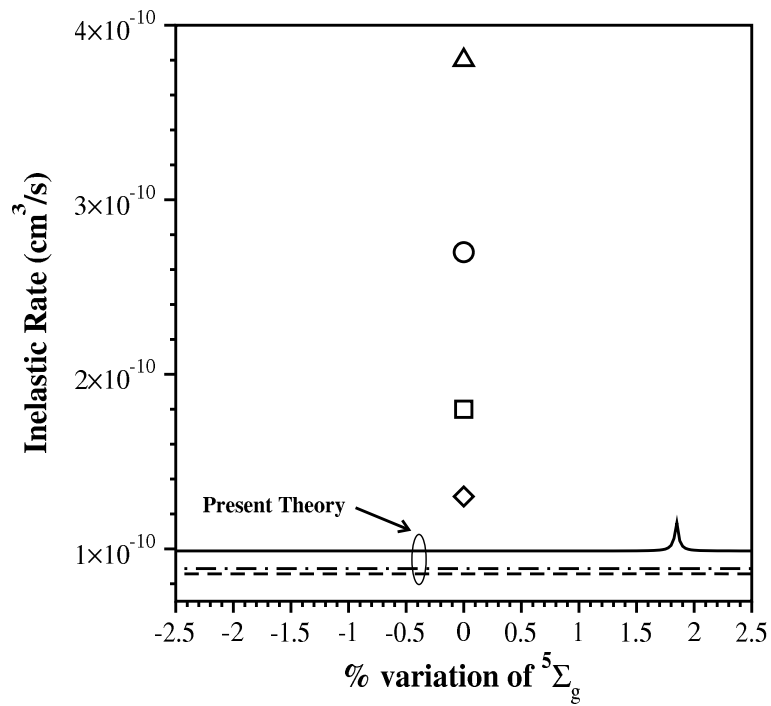


FIG. 8. Thermally-averaged Penning rates for an unpolarized gas with curves labeled as per Fig.5. The theoretical predictions possess an error of  $\approx 40\%$  and the experimental results have uncertainties on the order of 50%. Experimental results are denoted by  $\triangle$  for [21],  $\circ$  for [18],  $\square$  for [22] and  $\diamond$  for [26].